Research Square

Preprints are preliminary reports that have not undergone peer review.
They should not be considered conclusive, used to inform clinical practice,
or referenced by the media as validated information.

Molecular Dynamics Reveals the Mechanistic Basis for Peptide Inhibitor Evasion by the SARS-CoV-2 RBD ΔN487 Deletion

Zeinab Nazarian-Samani
Tarbiat Modares University
Shokouh Rezaei
Tarbiat Modares University
Saman Hosseinkhani
saman_h@modares.ac.ir
Tarbiat Modares University
Yahya Sefidbakht
Shahid Beheshti University

Article

Keywords: Peptide Design, SARS-CoV-2, Spike protein, receptor-binding domain (RBD), angiotensin-converting enzyme 2 (ACE2)

Posted Date: October 1st, 2026

DOI: https://doi.org/10.21203/rs.3.rs-9875328/v1

License: This work is licensed under a Creative Commons Attribution 4.0 International License.
Read Full License

Additional Declarations: No competing interests reported.

Molecular Dynamics Reveals the Mechanistic Basis for Peptide Inhibitor Evasion by the SARS-CoV-2 RBD ΔN487 Deletion

Zeinab Nazarian-Samani[1], Shokouh Rezaei[1], Saman Hosseinkhani[1*], Yahya Sefidbakht[2*]

[1]Department of Biochemistry, Faculty of Biological Sciences, Tarbiat Modares University, Tehran, Iran.

[2]Protein Research Center, Shahid Beheshti University, Tehran, Iran

*Corresponding authors: saman_h@modares.ac.ir[1], y_sefidbakht@sbu.ac.ir[2]

Abstract:

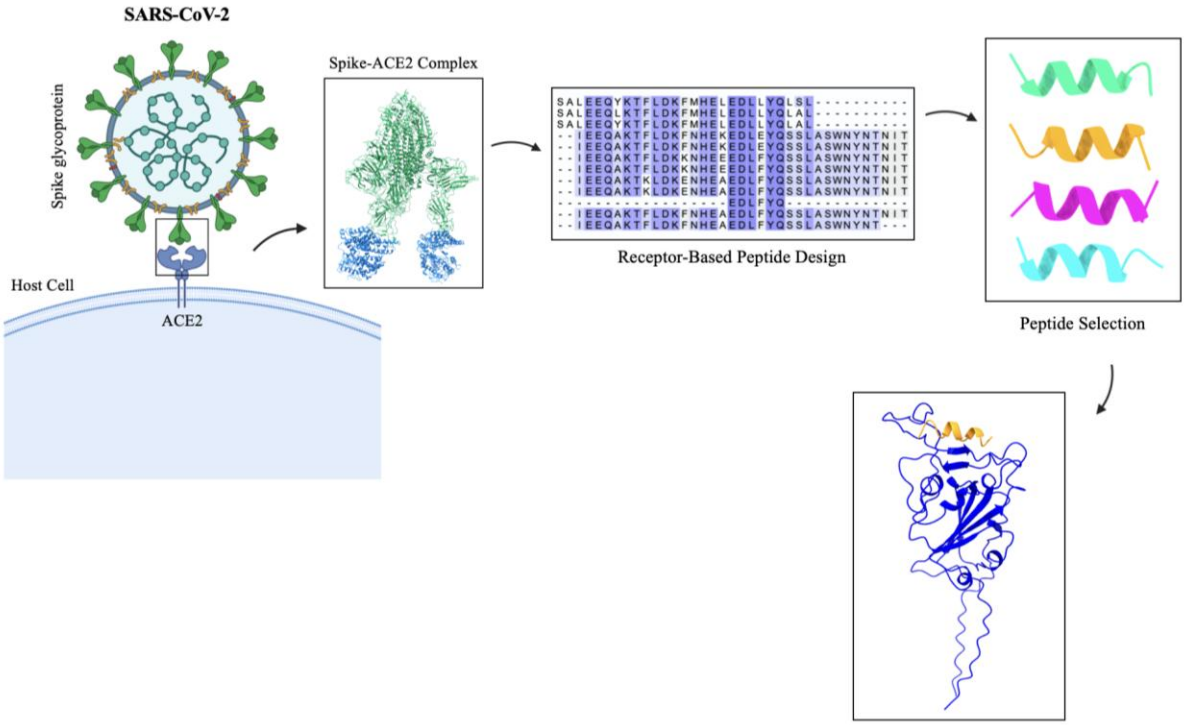
Mutational diversification within the SARS-CoV-2 receptor-binding motif (RBM) continues to reshape the local structural and physicochemical landscape of the receptor-binding domain (RBD), while largely preserving its global fold. Here, we present the first integrated structural and dynamical analysis of the N487 deletion (ΔN487) within the RBM in complex with an engineered ACE2-derived inhibitory peptide.

Using 100-ns all-atom molecular dynamics simulations combined with high-accuracy structural modeling, mutation-induced stability profiling, electrostatic potential mapping, and interaction-network analysis, we systematically evaluated how selected RBM mutations—including L452R, N487D, Q493E, and ΔN487—affect RBD conformation and peptide engagement.

Among the examined mutations, ΔN487 produced the most pronounced local rearrangements, inducing altered loop orientation, solvent exposure, and surface electrostatics without disrupting the global RBD architecture.

The ACE2-derived α-helical peptide maintained conformational stability and persistent α-helicity across native and mutant RBD complexes.

Together, these computational findings indicate that RBM deletions can reshape local binding microenvironments without compromising global RBD stability and establish a mechanistic framework for understanding deletion-driven vulnerabilities that may inform future experimental and biophysical validation of peptide-based inhibitors.



Key Words: Peptide Design; SARS-CoV-2; Spike protein; receptor-binding domain (RBD); angiotensin-converting enzyme 2 (ACE2)

Highlights:

-first structural and dynamical characterization of the N487 deletion (ΔN487) in the SARS CoV-2 RBM in complex with an ACE2-derived peptide .

-ΔN487 induces localized conformational and electrostatic remodeling while preserving global RBD stability .

-Deletion-driven microenvironmental changes create mutation-specific peptide-binding micro-hotspots.

-Interaction network analysis reveals mutation-dependent rewiring of stabilizing interfacial contacts.

-Findings provide mechanistic insight into mutation-tolerant peptide–RBD interactions.

1.Introduction

Since its emergence in late 2019, severe acute respiratory syndrome coronavirus 2 (SARS-CoV-2) has spread globally, causing the COVID-19 pandemic and substantial public-health and socioeconomic consequences [1]. Although vaccination strategies and therapeutic antibodies have significantly reduced disease severity, the continued evolution of the viral spike protein—particularly within the receptor-binding domain (RBD)—has progressively eroded the efficacy of several first-generation countermeasures [2].

The RBD (residues 319–541) mediates viral entry through direct interaction with the angiotensin-converting enzyme 2 (ACE2) receptor. Within the RBD, the receptor-binding motif (RBM; residues 438–506) forms the principal interface with ACE2 receptor and constitutes a hotspot for recurrent mutations that modulate receptor affinity, immune escape, and therapeutic susceptibility [3–5]. Most structural and computational investigations to date have focused predominantly on RBM substitutions, while the structural and functional consequences of RBM deletions remain comparatively underexplored. Peptide-based inhibitors targeting the RBD–ACE2 interface have emerged as a promising antiviral strategy due to their structural tunability, favorable safety profiles, and compatibility with rational design. Short ACE2-derived α-helical peptides have been shown to competitively bind the RBD and disrupt ACE2 engagement, with subsequent optimization efforts improving helicity, stability, and binding affinity [6]. These designs enhanced helicity, resistance to proteolysis, and binding affinity, in some cases reaching nanomolar activity in vitro.

In parallel, computationally designed miniproteins and fusion inhibitors have suggested potent antiviral activity in vitro and in vivo [7,8]. Despite these advances, the impact of ongoing RBM evolution on peptide–RBD interaction mechanisms remains incompletely understood, particularly in the context of newly emerging lineages.

The emergence of Omicron and its descendants have reshaped the RBM mutational landscape, introducing substitutions and deletions at key interface residues that compromise antibody neutralization and alter receptor engagement [15]. Global surveillance efforts by the World Health Organization and GISAID have classified these lineages as Variants of Concern (VOC), Variants of Interest (VOI), or Variants Under Monitoring (VUM) [16,17]. Recently identified VUMs, including NB.1.8.1 and XFG, harbor alterations at residue N487—including substitutions and deletions—that occupy a critical structural position within the RBM yet remain poorly characterized at the molecular level (table1) [18].

Table1: Mutations that play an important role in the interaction of RBD with ACE2

RBD mutation sites	Category	Alpha	Beta	Gamma	Delta	Omicron	BA.1	BA.2	XBB	XBB.1.5	NB.1.8.1	XFG	Potential Molecular Mechanism	Potential Clinical Consequences
Q493E	VUM/VOI										✓	✓	Substitutes a charged residue at the interface; effect context-dependent	Possible reduction in neutralization by some mAbs; modest effect on transmissibility.
L452R	VOC				✓						✓	✓	Enhances receptor interaction and reduces binding by several neutralizing antibodies.	Higher transmissibility (Delta, BA.4/5); reduced neutralization by vaccine sera.
T478V	VUM/VOI										✓		Hydrophobic substitution near ACE2 interface; specific effects context-dependent.	Unclear/limited evidence for major clinical impact.
N487D	VUM/VOI											✓	Alters a key ACE2 contact residue, usually decreasing affinity.	Likely fitness cost unless compensated by other mutations
N487del	VUM/VOI										✓		Deletion at this position disrupts local structure and ACE2 contacts.	Potential loss of fitness; context-dependent effects.
V445P	VUM/VOI											✓	Proline substitution can alter local backbone conformation affecting antibody epitopes.	Possible reduction in neutralization by some sera; limited data.

Notably, residue N487 serves as a key anchoring element within the RBM loop, contributing to ACE2 engagement and local structural organization. While substitutions at this position have been reported, the structural consequences of N487 deletion (ΔN487), particularly in the context of peptide inhibitor binding, have not been systematically investigated. This study provides the first integrated structural and dynamical characterization of the ΔN487 deletion within the SARS-CoV-2 RBM in complex with an engineered ACE2-derived inhibitory peptide. Through molecular dynamics simulations combined with stability profiling, electrostatic potential analysis, and interaction network mapping, we elucidate how mutation-induced local rearrangements reshape the RBM microenvironment and influence peptide accommodation. These findings offer mechanistic insight into mutation-tolerant peptide–RBD

interactions, providing a foundation for future experimental validation and rational inhibitor optimization.

2. Computational methods

2.1. Structure Prediction

The amino acid sequence of the RBD from the S protein sequence of SARS-CoV-2 sequence was retrieved from the UniProt database [19], under the identifier numbers of P0DTC2. The native RBD structure and its mutant variant models were predicted using the AlphaFold server (https://alphafoldserver.com), which provides high-accuracy 3D structure predictions based on deep learning [20].

2.1.1 Selection of Mutations

A435S**,** Q493E**,** T478V, and ΔN487 Mutations were identified as characteristic substitutions of the NB1.8.1 variant, while N487D, Q493E**,** V445P, and L452R mutations corresponded to the XFG variant, according to data obtained from the GISAID database (https://gisaid.org). To specifically evaluate the structural and functional impact of the N487 deletion (ΔN487), both in isolation and in combination with other substitutional mutations, two distinct NB1.8.1 models were constructed and designated as follows:

- $RBD^{NB1.8.1(\Delta N487)}$: variant containing only the N487 deletion.
- $RBD^{NB1.8.1}$: variant carrying the ΔN487 along with A435S**,** Q493E**,** and T478Vsubstitutions.

2.1.2 Calculation of ΔΔG (affinity and destabilizing)

DynaMut2 (https://biosig.lab.uq.edu.au/dynamut2/) was used to predict $\Delta\Delta G^{destabilization}$ and **Δ** Vibrational Entropy Energy for mutations. DynaMut2 [21] is a web server that combines graph-based signatures with two established normal mode approaches to analyze protein dynamics and predict the impact of mutations on protein stability and flexibility. It also provides tools for visualization and comprehensive analysis of protein motion via a freely accessible platform.

2.2 Peptide design and Toxicity prediction

Candidate inhibitory peptides were collected from the ACovPepDB database (https://i.uestc.edu.cn/ACovPepDB/). Peptides were filtered based on two main criteria: (i) hACE2 source and (ii) RBD as the designated target. All selected sequences were aligned using the UniProt alignment tool, with the α-helix region of ACE2 serving as the reference. After several rounds of screening, four peptides with the highest sequence identity to helix of ACE2 were selected for further evaluation. The potential cytotoxicity of the selected peptides was predicted using the ToxinPred web server (http://crdd.osdd.net/raghava/toxinpred/) .

2.3 Physicochemical and Structural Analysis of the Selected Peptide

The physicochemical parameters of the selected peptide, including molecular weight, theoretical pI, instability index, aliphatic index, and GRAVY, were calculated using

the ProtParam tool [22]. The helical wheel projection was generated via the NetWheels web server (http://lbqp.unb.br/NetWheels/), providing a visual representation of the peptide's amphipathic helical nature.

2.4 Molecular Docking Analysis

Molecular docking studies were conducted using the HADDOCK2.4 web server [23] to investigate the interaction patterns between the RBD of SARS-CoV-2 and the designed ACE2-derived peptides. Subsequently, the four selected peptides were individually docked with each of the RBD models (native and mutant variants) under identical docking parameters. The docking results were evaluated based on HADDOCK scores, and the binding affinities of the top-ranked complexes were further estimated using the PRODIGY server. Comparison of HADDOCK and PRODIGY results allowed identification of the peptide exhibiting the strongest binding affinity and the most favorable orientation at the RBDs interface, which was subsequently selected for molecular dynamics (MD) simulations.

2.5 MD simulations

Energy minimization and MD simulations were performed by GROMACS-v2024.6 utilizing the CHARMM36m force field [24]. The structures (PDB format) that produced by AlphaFold server was used as an input. Water box was created with at least 1 nm (10 Å) distances from the protein and complexes using the SPC water model and applying boundary conditions. The system neutralization was done by adding Na^+ and Cl^- ions at the concentration of 0.15 M.

The MD simulation was carried out to investigate the quality of the structures by checking their stability via performing 100 ns simulations at a constant temperature 310 K (NVT step). Energy minimization was performed in 50,000 steps to avoid any bad contacts generated while solvating the system. Then the NPT optimization was done for 100 ps. To increase the likelihood of achieving the appropriate structure, the MD simulation was performed for 100 ns. Finally, GROMACS package was applied for the trajectory analysis, including the parameters such as Root Mean Square Deviation (RMSD), Root Mean Square Fluctuation (RMSF), Radius of Gyration (R_g), and Solvent Accessible Surface Area (SASA).

2.6 Peptide–RBDs Interaction Analysis Using RING 3.0

To investigate the interactions between the selected peptide and the native or mutated RBD structures, we utilized the RING 3.0 [25]. For this purpose, PDB files extracted from the MD simulations of the peptide–RBD complexes were used as input. RING 3.0 identifies both covalent and non-covalent interactions at the atomic level, including hydrogen bonds, ionic interactions, van der Waals contacts, and π–π stacking interactions. This analysis provided detailed information on the specific atomic interactions between the peptide and the RBD, offering insights into the binding interface and the key residues involved, which were crucial for downstream interpretation and validation of peptide binding.

3. Results

3.1. Structural analysis of RBD motif

Figure 1 compare the superimposed structures of four different RBDs. The results of this study show that the deletion of the asparagine residue at position 487 (ΔN487)—marked by a red arrow in both panels—induces a localized conformational change (Figure 1a) within the RBM (Figure 1b). This critical region is responsible for direct interaction with the host cell receptor (hACE2). The observed conformational change in the RBM due to the deletion of N487 could directly affect the binding affinity of hACE2 and other molecules (such as peptides). This finding emphasizes the key structural role of residue N487 in maintaining the structural and functional integrity of the RBM region and suggests that mutations at this specific position could provide new interaction network.

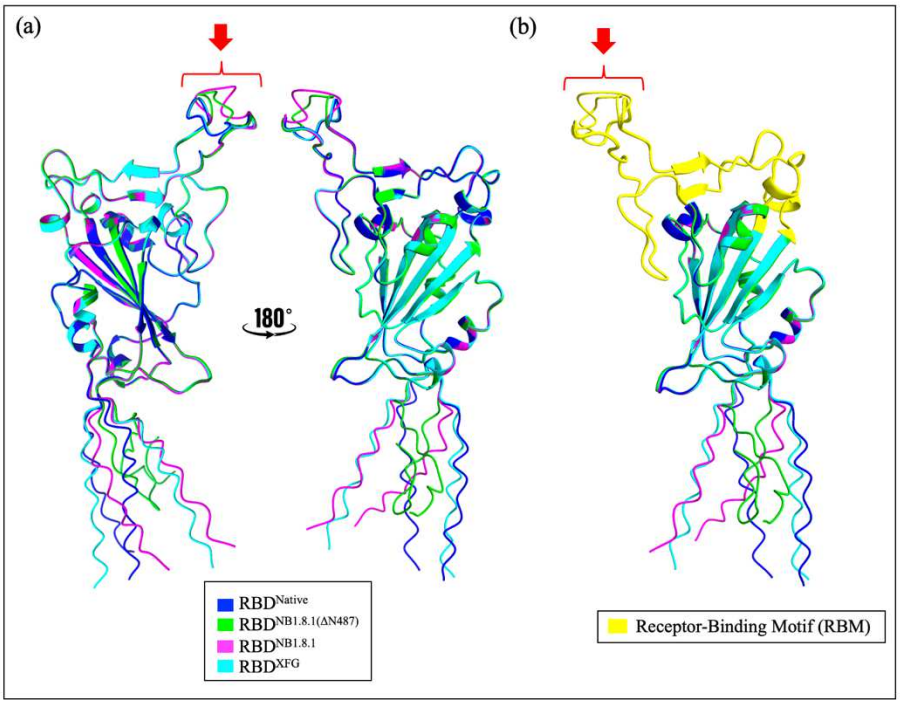


Figure 1: Superimposition of the RBDs of SARS-CoV-2

3.2. Effect of RBD mutations on thermodynamic parameters

Key RBD mutations, including N487D, V445P, L452R, A435S, Q493E, and T478V, were examined using the DynaMut server to determine their impact on structural stability and molecular flexibility. The results (Table 1) showed that some mutations, such as L452R and T478V, are associated with local structural stabilization and significant reduction in flexibility, possibly through the formation of new electrostatic interactions and hydrogen bonds, which restrict movement. Mutations such as V445P also showed a reduction in local flexibility, consistent with the stiffening nature of proline. In contrast, mutations such as N487D and Q493E have a relative or opposite effect on stability and flexibility, suggesting that their effect is limited to local regions or that they increase structural dynamics. Overall, these analyses

suggest that different RBD mutations can alter molecular behavior in different ways, from stabilizing the structure to increasing flexibility, and these differences are likely to have important consequences for interactions with ligands (such as peptides) or receptors.

Table 2: Predicted effects of key RBD mutations on $\Delta\Delta G^{Stability}$ and $\Delta\Delta S^{vib}$

Mutation	**ΔΔG**	**Δ Vibrational Entropy Energy**
N487D	0.001 kcal/mol (Stabilizing)	-0.008 kcal.mol^{-1}.K^{-1} (Decrease of molecule flexibility)
V445P	0.283 kcal/mol (Stabilizing)	-0.068 kcal.mol^{-1}.K^{-1} (Decrease of molecule flexibility)
L452R	0.193 kcal/mol (Stabilizing)	-0.197 kcal.mol^{-1}.K^{-1} (Decrease of molecule flexibility)
A435S	-0.520 kcal/mol (Destabilizing)	-0.223 kcal.mol^{-1}.K^{-1} (Decrease of molecule flexibility)
Q493E	-0.066 kcal/mol (Destabilizing)	0.182 kcal.mol^{-1}.K^{-1} (Increase of molecule flexibility)
T478V	0.779 kcal/mol (Stabilizing)	-0.384 kcal.mol^{-1}.K^{-1} (Decrease of molecule flexibility)

3.3. Electrostatic Surface Analysis of RBD Variants

Figure 2 illustrates the comparative electrostatic surface distribution of the RBD among different variants, highlighting the impact of single and multiple amino acid substitutions. In the RBD^{Native}, residues such as N487, L452, V445, T478, and Q493 exhibit a neutral-to-slightly polar character, contributing to a balanced charge distribution on the binding surface. Upon substitution with charged residues, substantial local electrostatic alterations become evident.

The N487D mutation introduces a negatively charged aspartate, shifting the local potential from neutral to electro-negative (red region), which may influence hydrogen bonding capacity and weaken interactions with positively charged residues on ACE2 and peptide.

Similarly, Q493E replaces a polar amide with an acidic carboxyl group, increasing the negative potential in this region and potentially altering receptor affinity and antibody recognition. In contrast, the L452R mutation introduces a positively charged arginine in a previously hydrophobic pocket, generating a pronounced electropositive area (blue region) that could enhance electrostatic complementarity with the negatively charged ACE2 and peptide surfaces.

The V445P mutation, while not directly altering charge, may rigidify the local structure, indirectly affecting the orientation of neighbouring charged residues. Likewise, T478V reduces polarity through the substitution of threonine with a hydrophobic valine, decreasing surface polarity and potentially modulating the hydrophobic interface.In the NB1.8.1 and XFG variants containing multiple concurrent substitutions, the cumulative effects of these charge redistributions are visible as extensive regions of polarized potential, suggesting synergistic modulation of the electrostatic landscape of RBD. These alterations likely affect both receptor/peptide binding and immune evasion through local perturbation of electrostatic complementarity and conformational flexibility at the binding interface.

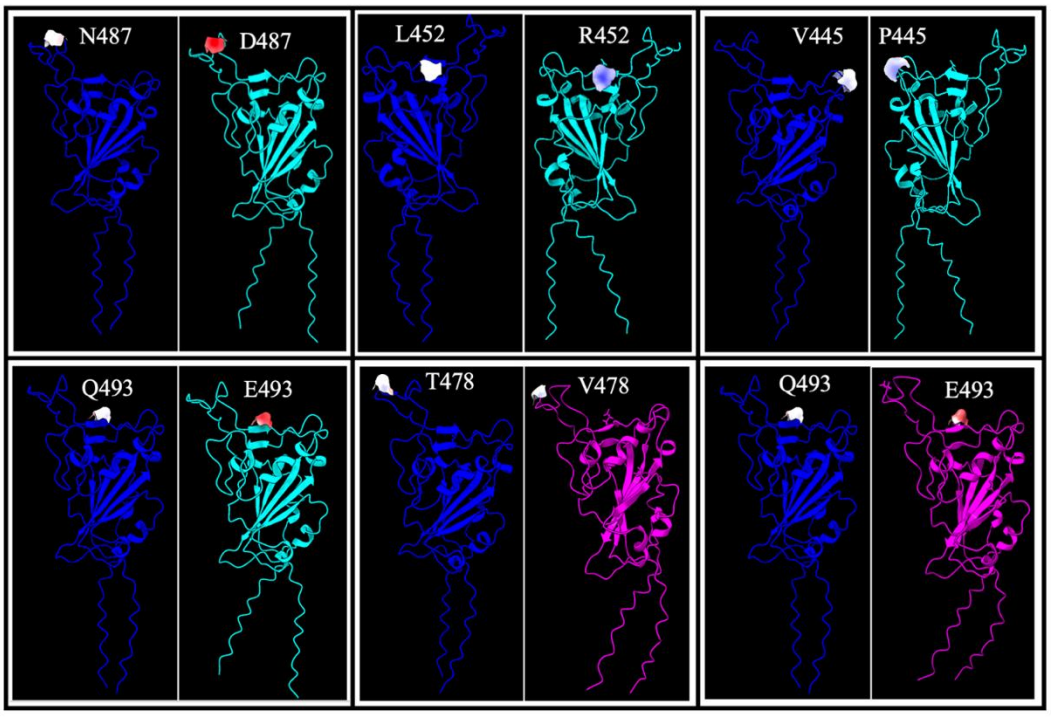


Figure 2: Effect of mutations on the electrostatic potential of RBD SARS-CoV-2. Blue and red represent positive and negative charges, respectively.

3.4. Designed peptide and its helical Wheel Representation

Based on main knowledge related to helical peptide structure, an inhibitory peptide which targeting ability against RBD-ACE2 interface were designed. The analyzed helix exhibits a clear amphipathic arrangement, with hydrophobic residues (F3, L10, and Y12) clustered on

one side of the helix, while polar and charged residues (D1, D9, E6, E11, K2, K7, and H5) are localized on the opposite side (Figure 3). This asymmetric distribution of polarity results in two distinct surfaces: a hydrophobic face likely involved in interactions with membranes or hydrophobic protein regions, and a polar face exposed to the aqueous environment. Such an arrangement highlights the amphipathic nature of the peptide, which is typically associated with enhanced structural stability and a propensity to participate in protein–protein or protein–membrane interactions.

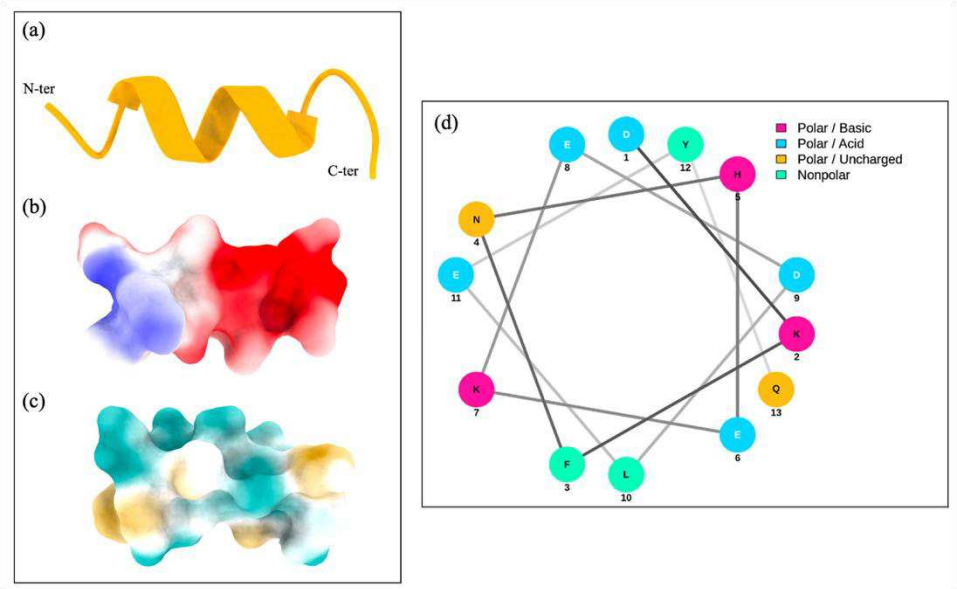


Figure 3: (a) 3D structure of a peptide, (b) electrostatic and (c) hydrophobic surfaces of peptide, (d) helical wheel projection showing the spatial arrangement of amino acids in the peptide.

3.5. In silico characterization of the designed Peptide

The designed peptide comprises 5 negatively charged residues (Asp + Glu) and 2 positively charged residues (Arg + Lys). Its atomic composition is C74H107N19O27, totaling 227 atoms. In silico characterization of the peptide shows it lacks tryptophan residues, resulting in a predicted extinction coefficient of 1490 $M^{-1}cm^{-1}$ at 280 nm, which may carry an error >10%. The estimated half-life of the peptide is 1.1 h in mammalian reticulocytes (in vitro), 3 min in yeast (in vivo), and over 10 h in *E. coli* (in vivo). The instability index (II) is 17.52, classifying the peptide as stable. The aliphatic index is 30.00, and the grand average of hydropathicity (GRAVY) is -2.323, indicating a highly hydrophilic nature.

3.6. MD simulation study

3.6.1. Analysis of free RBDs

To investigate the structural stability of RBDs during molecular dynamics simulations, the RMSD changes of C_α atoms in four different domains including RBD^{Native}, $RBD^{NB1.8.1(\Delta N487)}$, $RBD^{NB1.8.1}$ and RBD^{XFG} were investigated. The average RMSD values for these structures were 0.78 nm, 0.63 nm, 0.64 nm and 0.71 nm, respectively. At the beginning of the simulation, all structures showed a rapid increase in RMSD value, indicating the rearrangement of the structure and its adaptation to its surrounding environment (aqueous environment). As shown in Figure 4a, after about 10 to 15 ns, the RMSD curves reached a stable region, indicating the convergence of the simulation and the absence of extensive structural changes or significant unfolding of the protein.

The slight increase in the average R_g value of $RBD^{NB1.8.1(\Delta N487)}$ and $RBD^{NB1.8.1}$ (from 2.11 in RBD^{Native} to 2.17 and 2.16 nm, respectively) suggests that the deletion of N487 residue and the accompanying mutations slightly reduce the compactness of the RBD structure (Figure 4b). In contrast, the average R_g value of RBD^{XFG} is identical to that of RBD^{Native} (2.11 nm), implying comparable structural stability and compactness (Figure 4b). Overall, the differences in R_g values are minor (approximately 0.05–0.06 nm), indicating that none of the mutations caused notable unfolding or overall structural destabilization.

In order to investigate the changes in the contact area of different RBD structures with the solvent environment and to assess their compactness, the average SASA values were calculated during molecular dynamics simulations. The SASA value for the RBD^{Native} was obtained to be 137.33 nm^2 and was used as a basis for comparison. The SASA value of $RBD^{NB1.8.1(\Delta N487)}$ was 139.45 nm^2, indicating a slight increase in the contact area with the solvent. This increase could be due to the deletion of the N487 residue, which probably caused a local opening or increased flexibility in the adjacent regions. In contrast, the SASA value of $RBD^{NB1.8.1}$ was calculated to be 136.45 nm^2, which is a decrease compared to the $RBD^{NB1.8.1(\Delta N487)}$. This decrease may reflect the compensatory effect of new insertions that restore some of the structural compactness lost by the deletion. Finally, the RBD^{XFG} structure showed the lowest SASA value (135.19 nm^2), indicating higher compactness and reduced solvent exposure. This could be due to increased intramolecular interactions or greater stability of the folded structure.

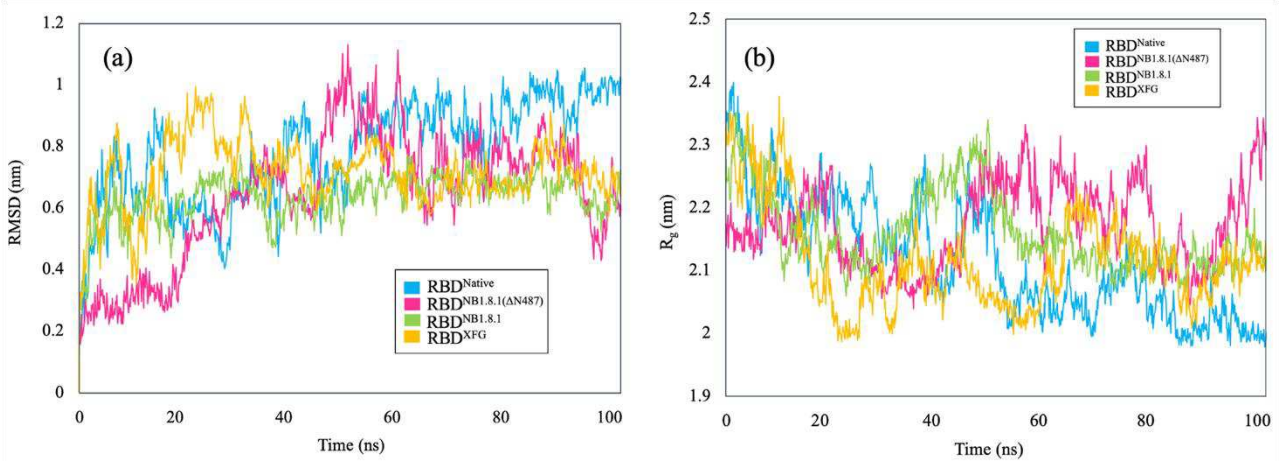
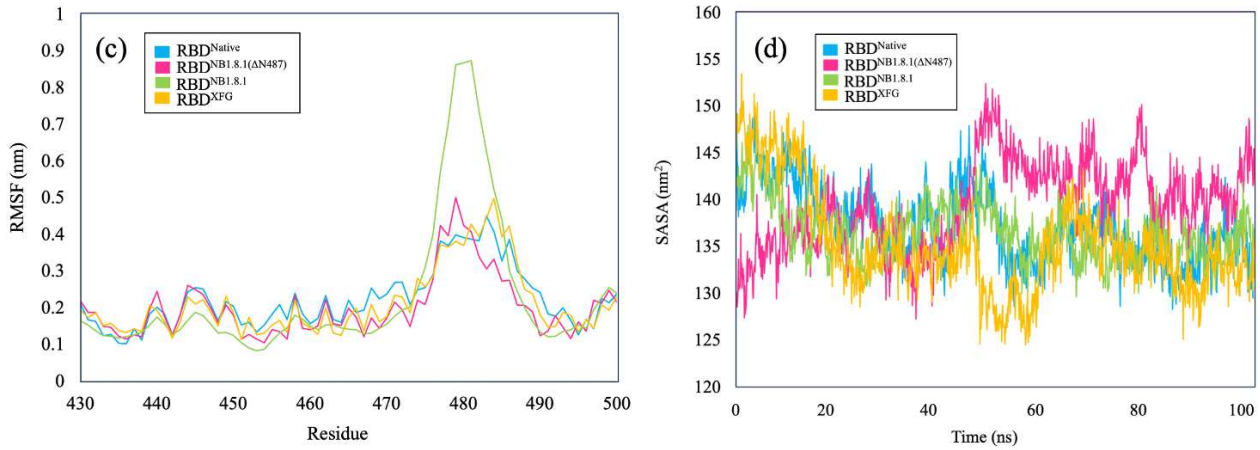


Figure 4: MD analysis of RBD structures during 100 ns.

3.6.2. Analysis of RBD-Peptide Complexes

As shown in Figure 5a, the RMSD plots revealed that the binding of the designed peptide generally made the RBD structures more stable compared to the free RBDs. For $RBD^{NB1.8.1(\Delta N487)}$, the RMSD decreased from 0.63 nm (free RBD) to 0.46 nm in the complex, indicating a very stable interaction and that the peptide effectively constrained the flexibility of the RBD. In contrast, $RBD^{NB1.8.1}$, which has several additional insertion mutations in



addition to ΔN487, showed a moderate RMSD decrease from 0.64 nm to 0.55 nm upon peptide binding, indicating a relatively stable complex with a slight increase in the mobility of the RBD and peptide. These results indicate that the deletion of N487 residue plays a major role in stabilizing the peptide, while the additional insertions slightly reduce the stability of the complex. For RBD^{XFG}, the RMSD of free RBD was 0.71 nm and increased to 0.74 nm in the presence of peptide.

On the other hand, peptide RMSD analysis showed that the degree of peptide movement and stabilization in complex with different mutant RBDs varied (Figure 5b). In the complex with $RBD^{NB1.8.1(\Delta N487)}$, the peptide RMSD was only 0.25 nm, indicating a very high stability of the peptide and its fixed positioning on the RBD surface. This suggests that the deletion of N487 residue likely created a favorable binding site for the peptide and enhanced the interaction of the complex.

Overall, the MD simulation results showed that the designed peptide was able to effectively stabilize all RBDs. While the complex with $RBD^{NB1.8.1(\Delta N487)}$ showed the highest stability, the other two mutants, namely $RBD^{NB1.8.1}$ and RBD^{XFG}, had RMSD values close to native RBD despite the mutational changes. This indicates that in addition to stabilizing ΔN487 residue, the peptide can also inhibit these mutants well and the interaction of the peptide with RBDs is relatively stable and effective. Therefore, the peptide design has great potential to target several different RBD mutants and can act as a specific binder or inhibitor.

The R_g of the different RBD–peptide complexes showed that the changes in compactness in each of the variants had a different pattern (as shown in Figure 5c and d). In the $RBD^{NB1.8.1(\Delta N487)}$ complex, the R_g value of the RBD structure remained unchanged compared to the free form (2.17 to 2.17 nm). In contrast, the R_g value of the peptide in this complex was 0.73 nm, which is the lowest value among all groups. In other words, the deletion of the N487 residue probably created a suitable binding pocket in which the peptide is anchored tightly and stably.

In the $RBD^{NB1.8.1}$, the R_g of RBD increased from 2.16 to 2.22 nm, which is the largest increase among the other groups. The R_g of the peptide in this complex is also 0.85 nm. These changes indicate a relative decrease in compactness and the occurrence of a local opening in the RBD structure upon peptide binding. It seems that the insertion mutations have changed the geometry of the binding site, which has led to a decrease in the overall stability of the complex. In the RBD^{Native}–peptide complex, the R_g of RBD showed only a slight increase from 2.11 to 2.14 nm, while the R_g of the peptide has the highest value (0.89 nm). These data indicate that the peptide is relatively open and flexible on the RBD^{Native} surface, without being embedded in a deep pocket. Therefore, the complex of RBD^{Native} and peptide is less stable and compact than the $RBD^{NB1.8.1(\Delta N487)}$-peptide complex. As shown in Figure 5c, the RBD^{XFG} behaved similarly to the native form, with the R_g of RBD in the complex remaining almost constant (from 2.11 to 2.12 nm) and the R_g of the peptide being moderate (0.84 nm) (Figure 5d). These results indicate that RBD^{XFG} maintains its overall structure and the peptide remains somewhat more compact and stable compared to the native form, although this stability is not as significant as that of the $RBD^{NB1.8.1(\Delta N487)}$-peptide complex.

To investigate the effect of peptide binding on the structural features and compactness of the different RBD domains, the average SASA values were calculated for each complex and its components.

In the native RBD, the SASA value was 137.33 nm^2, while in its complex with the peptide, the SASA value of RBD decreased to 137.05 nm^2. This slight decrease indicates that peptide binding causes a slight decrease in the contact of RBD with the solvent and an increase in the local compactness at the binding site. The SASA value of the peptide in this complex is also 20.23 nm^2, indicating a significant involvement of part of its surface in the interaction with RBD.

The SASA value of $RBD^{NB1.8.1(\Delta N487)}$ in the free state was 139.45 nm^2 and in the complexed state was 136.14 nm^2. This more pronounced decrease compared to the native RBD suggests that the deletion of N487 increased the surface area of the RBD to form more stable contacts with the peptide. At the same time, the amount of SASA of the peptide in this complex (17.66 nm^2) also decreased, indicating that more surface area of the peptide was covered by the binding to the RBD. In the $RBD^{NB1.8.1}$, the amount of SASA increased from 136.45 nm^2 in the free state to 138.38 nm^2 in the complexed state. This increase could be due to the change in surface arrangement due to the new insertions, which led to a rearrangement of the structure and increased surface contacts with the solvent during peptide binding. The amount of SASA

of the peptide in this complex was also 19.75 nm^2, indicating a balanced surface contact between the peptide and the RBD.

Finally, the RBD^{XFG} variant showed the lowest SASA value among the samples; it decreased from 135.19 nm^2 in the free state to 134.05 nm^2 in the complexed state. This decrease indicates a higher compactness and probably higher stability of the complex. The SASA value of the peptide in this state (19.41 nm^2) was also close to the other states, indicating that the surface contact of the peptide with the RBD is relatively similar.

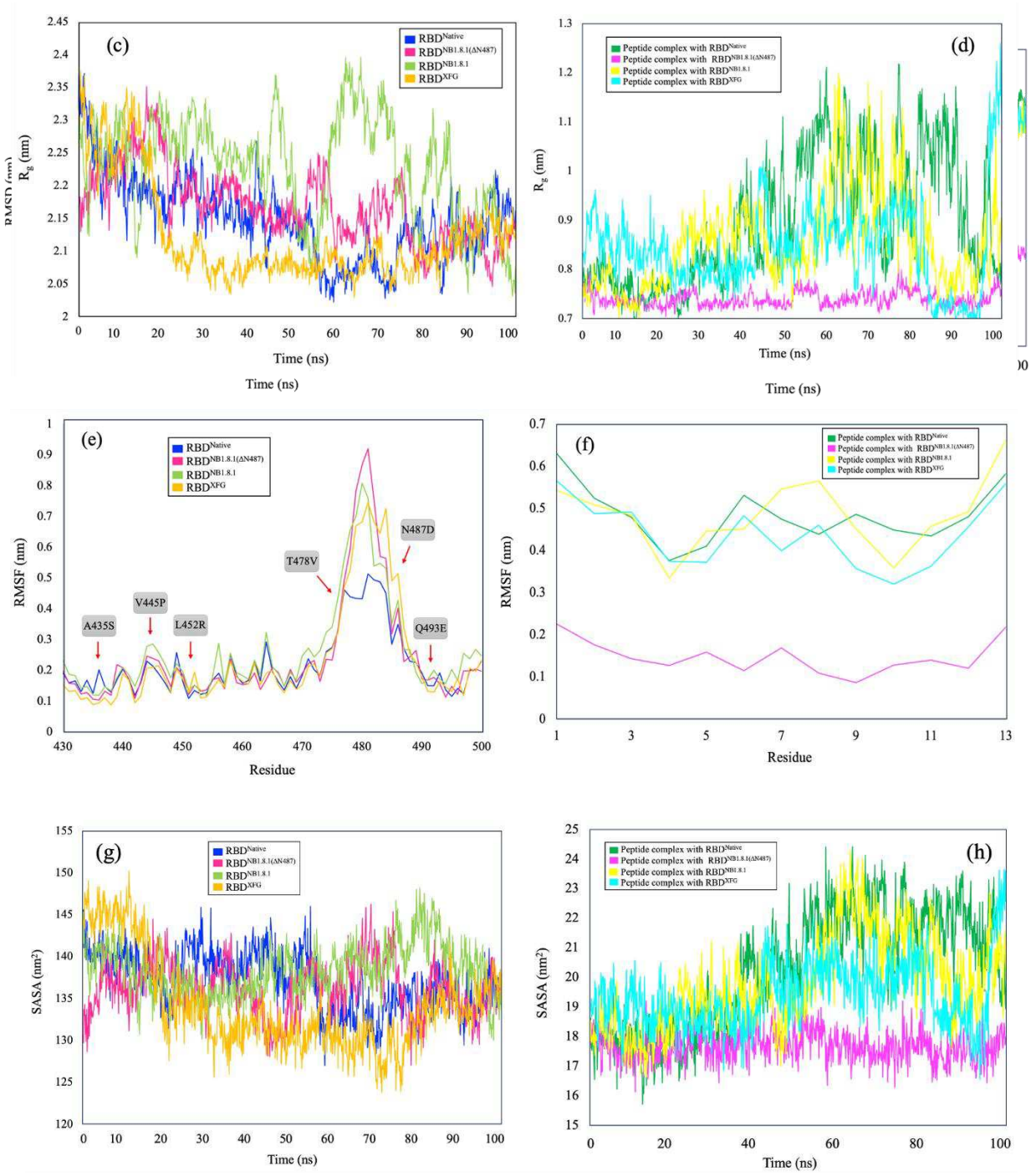


Figure 5: MD analysis of RBD-Peptide complexes during 100 ns.

7.RBD-peptide interactions

The number of H-bonds between the designed peptide and RBD (Native and Mutant structures) showed that the RBD^{Native}-peptide and the $RBD^{NB1.8.1(\Delta N487)}$-peptide complexes (Table 3 and 4) both have four H-bonds, while in the $RBD^{NB1.8.1}$-peptide complex reduced to three (Table 5) and in the RBD^{XFG}-peptide complex to two (Table 6). This trend indicates a gradual decrease in hydrogen interactions in the mutated variants compared to the native structure.

When comparing the π–π interactions between the peptide and the RBDs (native and mutants), a significant difference was observed in the number and position of these interactions. In the RBD^{Native}-peptide complex, there was only one π–π interaction between a tyrosine residue of the peptide and one of the aromatic residues of the RBD (Table 3). In the $RBD^{NB1.8.1(\Delta N487)}$-peptide complex, the number of these interactions increased to two (Tyr12–Tyr453 and Tyr12–Tyr494) (Table 4), probably indicating the formation of new aromatic interactions in response to the local conformational change caused by the N487 deletion. In the $RBD^{NB1.8.1}$-peptide complex, only one π–π interaction (Tyr12–Tyr449) was observed (Table 5), which was reduced compared to the N487del state. While in the RBD^{XFG}-peptide complex, a different π–π interaction was formed between Phe3 of the peptide and Phe486 of the RBD, indicating a shift in the location of the aromatic interactions compared to the other species.

The investigation of π-cation interactions between the peptide and different RBD variants showed that this type of interaction is limited in distribution among complexes. No π-cation interactions were observed in the RBD^{Native}-peptide and $RBD^{NB1.8.1}$-peptide complexes. In contrast, in the $RBD^{NB1.8.1(\Delta N487)}$-peptide complex, a π-cation interaction was formed between Tyr12 of the peptide and Tyr403 of the RBD (Table 4), indicating a local rearrangement at the binding surface. As well as, in the RBD^{XFG} -peptide complex, a novel interaction was identified between Lys7 of the peptide and Phe490 of the RBD.

Ionic interactions between the peptide and the different RBDs showed that this type of interaction was more common in the mutant structures than in the native RBD. No ionic interactions were formed in the RBD^{Native}, whereas in the $RBD^{NB1.8.1(\Delta N487)}$-peptide complex two ionic interactions were formed between Gln8–Lys417 and Glu11–Lys417 (Table 4). This may indicate the presence of positively charged sites in the mutant RBD that are able to attract polar and charged residues of the peptide.

In the $RBD^{NB1.8.1}$-peptide complex, an ionic interaction was formed between Lys2 of the peptide and Glu484 of the RBD, and in the RBD^{XFG}-peptide complex a similar interaction was observed between Lys7 and Glu484. In general, mutated variants establish more ionic interactions than the native structure, which can affect the stability and how the peptide is positioned on the RBD surface.

VDW interactions between the peptide and the RBDs are conserved in all complexes, and no significant change in the total number of these contacts is observed. These steric interactions play an important role in the stability and conformation of the peptide–RBD complexes, and details of each contact are provided in Tables 3–6.

Table 3: Molecular interactions between RBD^{Native} and peptide.

Interactions	**Peptide**	**RBD**
H-Bonds	ASP1	TYR489
	LYS2	GLN493
	TYR12	ASN501
	GLN13	TYR505
π-π Stack	TYR12	TYR505
VDW	ASP1	TYR489
	LYS2	TYR489
	TYR12	ASN501

Table 4: Molecular interactions between $RBD^{NB1.8.1(\Delta N487)}$ and peptide

Interaction	**Peptide**	**$RBD^{NB1.8.1}$**
H-Bonds	GLU8	LYS417
	GLU11	LYS417
	TYR12	GLU406
		TYR494
π-π Stack	TYR12	TYR453
		TYR494
π-Cation		ARG403

Ionic	GLU8	LYS417
	GLU11	LYS417
VDW	ASP9	LEU455
	GLU11	LYS417
	TYR12	ILE418
		TYR453

Table 5: Molecular interactions between $RBD^{NB1.8.1}$ and peptide.

Interactions	**Peptide**	**$RBD^{NB1.8.1}$**
H-Bonds	GLU6	GLY485
	LYS7	GLU492(3)
	GLN13	TYR449
π-π Stack	TYR12	TYR449
Ionic	LYS2	GLU484
VDW	PHE3	VAL483 PHE486
	LYS7	LEU455 TYR488 PHE489

Table 6: Molecular interactions between RBD^{XFG} and peptide

Interaction	**Peptide**	**RBD^{XFG}**
H-Bonds	LYS7	GLU484
	GLU11	ARG452
π-π Stack	PHE3	PHE486
π-Cation	LYS7	PHE490
Ionic		GLU484
VDW	ASN4	VAL483
	LYS7	GLU484
		PHE490
	GLU11	ARG452
	TYR12	TYR449

.

4. Discussion

Consistent with previous studies, the SARS-CoV-2 RBD retains a conserved global fold despite RBM mutations, while functional effects arise primarily from localized structural perturbations. Our structural analyses showed that, although mutations cluster within the receptor-binding motif (RBM), they do not dramatically disrupt the overall fold of the RBD (Figure 1). Instead, changes tend to be accommodated by surface loops that can flexibly adjust without undermining the core architecture. This resilience in the RBD structure echoes observations from several structural studies, where even heavily mutated variants maintain a stable β-sheet core while surface residues adapt to new interaction patterns [26]. Such behavior likely reflects evolutionary pressure to preserve the functional core of the spike protein while permitting peripheral adjustments that modulate interaction with receptors or antibodies.

When we examined changes in thermodynamic parameters across variants (Table 2), a clear pattern emerged: single substitutions rarely act independently. Some mutations that might be expected to destabilize local packing instead co-occur with compensatory interactions elsewhere, resulting in an overall energetic balance. This aligns with results from robust computational and experimental efforts showing that variants such as those in the Delta and Omicron lineages can sustain a high mutational load without collapsing the RBD's stability [27]. In fact, increases in binding free energy upon mutations like L452R and T478K have been attributed to enhanced non-covalent interactions at the interface, highlighting how local destabilization may be offset by adaptive contacts.

Our electrostatic surface analyses revealed significant redistribution of local charge patterns in mutated RBDs (Figure 2). Substitutions such as N487D and Q493E reoriented surface charge in ways that altered potential interaction hotspots. Similar findings have been reported in detailed electrostatic investigations of SARS-CoV-2 variants, where changes in charge complementarity were shown to modulate both receptor and inhibitor engagement [28]. Notably, L452R — despite being distal to the canonical ACE2 interface — was observed in prior work to shift electrostatic landscapes favorably in certain mutational combinations, suggesting a nuanced role where electrostatic tuning can either strengthen or weaken specific contacts depending on context.

In designing our inhibitory peptide, we adopted an amphipathic α-helical scaffold intended to mirror key contact features of ACE2 (Figure 3). The resulting helical wheel emphasizes how hydrophobic residues project toward predicted RBM cavities while polar and charged side chains face outward toward solvent and potential electrostatic partners. This design is consistent with broader strategies in peptide inhibitor development, where pre-organized secondary structures have been leveraged to achieve both structural robustness and adaptable binding [29]. Past work on ACE2-mimetic peptides has demonstrated that maintaining helical integrity can be crucial for effective competition with receptor interactions.

Before considering interactions with the RBD, we characterized the peptide in isolation (Figure 3).

The peptide maintained a stable α-helical conformation throughout in silico sampling, suggesting that its secondary structure is inherently robust. Such pre-folded conformations are known to reduce the entropic penalty upon binding and have been linked to enhanced mutation tolerance in other viral inhibitory peptides [30]. In this sense, the peptide's intrinsic stability may underlie its capacity to engage diverse RBM variants without requiring significant structural rearrangement.

The molecular dynamics simulations suggest that none of the introduced mutations markedly disrupt the overall structural stability of the RBD. As shown in Figure 4a, all systems reach stable RMSD values shortly after the initial equilibration period, indicating that the observed fluctuations mainly reflect structural adaptation to the aqueous environment rather than unfolding. Similar RMSD behavior has been reported in previous computational studies of RBD variants, where mutations within the receptor-binding motif were found to alter local dynamics while leaving the global fold intact [31,32].

Subtle differences in global compactness are evident from the radius of gyration analysis (Figure 4b). The slightly higher Rg values observed for $RBD^{NB1.8.1(\Delta N487)}$ and $RBD^{NB1.8.1}$ point to a modest loosening of the structure, which may arise from increased flexibility in surface-exposed regions following residue deletion and mutation. Comparable trends have been described in earlier MD studies, where RBM modifications led to small increases in Rg and solvent exposure without compromising structural integrity [33]. In contrast, the RBD^{XFG} variant maintains an Rg value comparable to that of the native RBD, consistent with reports showing that certain mutation combinations can preserve or even reinforce structural compactness through stabilizing intramolecular interactions [34]. Overall, these observations support the notion that RBD mutations primarily fine-tune flexibility and solvent accessibility rather than inducing substantial structural rearrangements.

Peptide binding stabilizes RBD variants in a mutation-dependent manner. In $RBD^{NB1.8.1(\Delta N487)}$, RMSD drops markedly (Fig. 4C), reflecting tight peptide anchoring and restrained RBD motion, consistent with prior reports of deletion-induced rigidity [31,33]. Insertion mutations in $RBD^{NB1.8.1}$ produce only modest stabilization, likely due to interface alterations [34].

Rg and SASA analyses support these trends: ΔN487 promotes compactness and reduced flexibility (Fig. 4D–F), whereas insertion mutations allow partial opening. Native and RBD^XFG complexes exhibit intermediate behavior, indicating stable yet less confined binding [32,35]. Overall, N487 deletion optimizes peptide engagement through tighter packing and enhanced interface burial, highlighting its potential as a broadly effective RBD binder.

Intermolecular interactions between the designed peptide and RBD variants were mutation-dependent. H-bonds decreased from four in RBD^{Native} and $RBD^{NB1.8.1(\Delta N487)}$ (Tables 3–4) to three and two in $RBD^{NB1.8.1}$ and RBD^{XFG} (Tables 5–6). Mutations also remodeled π–π and π-cation contacts, with ΔN487 introducing new aromatic (Tyr12–Tyr453/Tyr494) and π-cation (Tyr12–Tyr403) interactions, while insertions shifted contact sites. Ionic interactions emerged mainly in mutants, whereas VDW contacts remained conserved, indicating that mutations subtly reshape the peptide-binding interface without disrupting steric stability. These trends

agree with prior studies linking RBD mutations to altered hydrogen bonding, aromatic contacts, and surface charge [31-33,35] and are supported by our data (Tables 3–6).

Together, these results indicate that RBM evolution does not uniformly erode inhibitor binding but can instead generate mutation-specific microenvironments that remain compatible with, or even favorable to, peptide engagement. While the present conclusions are derived from computational analyses and require experimental validation, this study establishes a conceptual framework for understanding how deletion-driven RBM remodeling can simultaneously support viral adaptation and create exploitable inhibitory vulnerabilities.

5.Conclusion

Overall, this study provides the first structural and dynamical analysis of the N487 deletion (ΔN487) within the SARS-CoV-2 receptor-binding motif in complex with an ACE2-derived inhibitory peptide. Molecular dynamics simulations indicate that ΔN487 induces localized conformational and electrostatic remodeling of the RBM while preserving the global structural stability of the RBD.

Deletion-driven microenvironmental rearrangements generate mutation-specific interaction micro-hotspots that support stable peptide binding across native and mutant RBD variants. Interaction network analysis further reveals mutation-dependent rewiring of hydrogen bonding, aromatic stacking, and ionic interactions, providing a mechanistic basis for mutation-tolerant peptide–RBD recognition.

Together, these computational findings establish a concise structural framework for understanding how RBM deletions can simultaneously preserve viral fitness and create exploitable binding vulnerabilities, supporting future experimental and biophysical validation of ACE2-derived peptide inhibitors.

Acknowledgment:

Financial support of this work is provided by a grant from of Tarbiat Modares University. (Grant# 58765).

Authors' contribution :

Conceptualization: Saman Hosseinkhani, Yahya Sefidbakht

Data curation: Shokouh Rezaei, Yahya Sefidbakht

Formal analysis: Zeinab Nazarian-Samani, Yahya Sefidbakht

Funding acquisition: Saman Hosseinkhani, Yahya Sefidbakht

Investigation: Shokouh Rezaei, Zeinab Nazarian-Samani

Methodology: Saman Hosseinkhani, Yahya Sefidbakht

Project administration: Saman Hosseinkhani, Yahya Sefidbakht

Resources: Saman Hosseinkhani , Yahya Sefidbakht

Software: Shokouh Rezaei, Zeinab Nazarian-Samani

Supervision: Saman Hosseinkhani, Yahya Sefidbakht

Validation: Saman Hosseinkhani, Yahya Sefidbakht

Visualization: Shokouh Rezaei

Writing–original draft: Zeinab Nazarian-Samani

Writing–review & editing: Saman Hosseinkhani, Yahya Sefidbakht

Declaration of generative AI and AI-assisted technologies in the writing process:

During the preparation of this work the author used SCISPACE(https://www.scispace.com), Gemini(https://www.gemini.com) in order to grammar correction, spelling mistakes, and sometimes paraphrasing the text to improve writing style.After using this tool/service, the authors reviewed and edited the content as needed and takes full responsibility for the content of the published article.

Data availability statement

The datasets used and/or analysed during the current study are available from the corresponding author on reasonable request.

References

1.Zhu N, Zhang D, Wang W, Li X, Yang B, Song J, et al.A novel coronavirus from patients with pneumonia in China, 2019.N Engl J Med. 2020;382(8):727733.doi:10.1056/NEJMoa2001017.

2.Planas D, Saunders N, Maes P, Guivel-Benhassine F, Planchais C, Buchrieser J, et al. Considerable escape of SARS-CoV-2 Omicron to antibody neutralization.Nature. 2022;602:671–675.doi:10.1038/s41586-021-04389-z.

3.Lan J, Ge J, Yu J, Shan S, Zhou H, Fan S, et al.Structure of the SARS-CoV-2 spike receptor-binding domain bound to the ACE2 receptor.Nature. 2020;581(7807):215–220. doi: 10.1038/s41586-020-2180-5.

4.Starr TN, Greaney AJ, Hilton SK, Ellis D, Crawford KHD, Dingens AS, et al.Deep mutational scanning of SARS-CoV-2 receptor binding domain reveals constraints on folding and ACE2 binding.Cell. 2020;182(5):1295–1310.e20.

5.Cao Y, Yisimayi A, Jian F, Song W, Xiao T, Wang L, et al.BA.2.12.1, BA.4 and BA.5 escape antibodies elicited by Omicron infection.Nature. 2022;608:593–602.doi:10.1038/s41586-022-05053-w.

6.Zhang G, Pomplun S, Loftis AR, Tan X, Loas A, Pentelute BL. Investigation of ACE2 N-terminal fragments binding to SARS-CoV-2 spike RBD. bioRxiv. 2020. doi: 10.1101/2020.03.19.999318.

7.Cao L, Goreshnik I, Coventry B, Case JB, Miller L, Kozodoy L, et al. De novo design of picomolar SARS-CoV-2 miniprotein inhibitors. Science. 2020;370(6515):426–431. doi: 10.1126/science.abd9909.

8.Xia S, Liu M, Wang C, Xu W, Lan Q, Feng S, et al. Inhibition of SARS-CoV-2 infection by a highly potent pan-coronavirus fusion inhibitor targeting its spike protein. Cell Res. 2020;30:343–355. doi:10.1038/s41422-020-0305-x.

9.Eberle RJ, Olivier DS, Amaral MS, Gadelha AP, Azevedo RC, Oliveira AC, et al. All-D-peptide inhibitors of the SARS-CoV-2 main protease. Nat Commun. 2021;12:5897. doi:10.1038/s41467-021-26193-0.

10-Báez-Santos YM, St John SE, Mesecar AD. The SARS-coronavirus papain-like protease: Structure, function and inhibition by designed antiviral compounds. Antiviral Res. 2015;115:21–38. doi:10.1016/j.antiviral.2014.12.015.

11.Rut W, Groborz K, Zhang L, Sun X, Zmudzinski M, Pawlik B, et al. SARS-CoV-2 Mpro inhibitors and activity-based probes for patient-sample imaging. Nat Chem Biol. 2021;17(2):222–228. doi:10.1038/s41589-020-00689-z.

12.Heitmann JS, Bilich T, Tandler C, Nelde A, Maringer Y, Marconato M, et al. A COVID-19 peptide vaccine for the induction of SARS-CoV-2 T cell immunity. Nature. 2021;590:152–157. doi:10.1038/s41586-020-3037-9.

13.Eberle RJ, Olivier DS, Amaral MS, Gadelha AP, Azevedo RC, Oliveira AC, et al. All-D-peptide inhibitors of the SARS-CoV-2 main protease. Nat Commun. 2021;12:5897. doi: 10.1038/s41467-021-26193-0.

14.Báez-Santos YM, St John SE, Mesecar AD. The SARS-coronavirus papain-like protease: Structure, function and inhibition by designed antiviral compounds. Antiviral Res. 2015;115:21–38. doi:10.1016/j.antiviral.2014.12.015.

15.Rut W, Groborz K, Zhang L, Sun X, Zmudzinski M, Pawlik B, et al. SARS-CoV-2 Mpro inhibitors and activity-based probes for patient-sample imaging. Nat Chem Biol. 2021;17(2):222–228. doi:10.1038/s41589-020-00689-z.

16.Heitmann JS, Bilich T, Tandler C, Nelde A, Maringer Y, Marconato M, et al. A COVID-19 peptide vaccine for the induction of SARS-CoV-2 T cell immunity. Nature. 2021;590:152–157. doi:10.1038/s41586-020-3037-9.

17. GISAID.Tracking of variants under monitoring (VUM) [Internet]. GISAID; 2023. Available from: https://www.gisaid.org.

18.Callaway E. Heavily mutated coronavirus variant puts scientists on alert. Nature. 2023;616:463–464. doi:10.1038/d41586-023-00868-1.

19.The UniProt Consortium. UniProt: the Universal Protein Knowledgebase in 2023. Nucleic Acids Res. 2023;51(D1):D523–D531. doi:10.1093/nar/gkac1052.

20.Jumper J, Evans R, Pritzel A, Green T, Figurnov M, Ronneberger O, et al. Highly accurate protein structure prediction with AlphaFold. Nature. 2021;596(7873):583–589. doi:10.1038/s41586-021-03819-2.

21.Rodrigues CHM, Pires DEV, Ascher DB. DynaMut2: Assessing changes in stability and flexibility upon single and multiple point missense mutations. Protein Sci. 2021;30(1):60–69. doi:10.1002/pro.3942.

22.Gasteiger E, Hoogland C, Gattiker A, Duvaud S, Wilkins MR, Appel RD, et al. Protein identification and analysis tools on the ExPASy server. In: The Proteomics Protocols Handbook. Springer; 2005. p. 571–607. doi:10.1385/1-59259-890-0:571.

23.Honorato RV, Trellet ME, Jiménez-García B, Schaarschmidt JJ, Giulini M, Reys V, et al. The HADDOCK2.4 web server for integrative modeling of biomolecular complexes. Nat Protoc. 2024;19(11):3219–3241. doi:10.1038/s41596-024-00928-2.

24.Huang J, Rauscher S, Nawrocki G, Ran T, Feig M, de Groot BL, et al. CHARMM36m: an improved force field for folded and intrinsically disordered proteins. Nat Methods. 2017;14(1):71–73. doi:10.1038/nmeth.4067.

25.Clementel D, Del Conte A, Monzon AM, Camagni GF, Minervini G, Piovesan D, et al. RING 3.0: fast generation of probabilistic residue interaction networks from structural ensembles. Nucleic Acids Res. 2022;50(W1):W651–W656. doi:10.1093/nar/gkac402.

26 .Walls AC, Park YJ, Tortorici MA, Wall A, McGuire AT, Veesler D. Structure, function, and antigenicity of the SARS-CoV-2 spike glycoprotein. Cell. 2020;181(2):281–292.e6. doi:10.1016/j.cell.2020.02.058.

27 .Motozono C, Toyoda M, Zahradnik J, Ikeda T, Saito A, Tan TS, et al. SARS-CoV-2 spike L452R variant evades cellular immunity and increases infectivity. Cell Host Microbe. 2021;29(7):1124–1136.e11. doi:10.1016/j.chom.2021.06.006.

28 .Barnes CO, Jette CA, Abernathy ME, Dam KA, Esswein SR, Gristick HB, et al. SARS-CoV-2 neutralizing antibody structures inform therapeutic strategies. Nature. 2020;588(7839):682–687. doi:10.1038/s41586-020-2852-1

29 .Zhang G, Pomplun S, Loftis AR, Loas A, Pentelute BL. Investigation of ACE2-derived peptide inhibitors of SARS-CoV-2. J Am Chem Soc. 2021;143(25):9326–9332. doi:10.1021/jacs.1c01006.

30 .Huang Y, Yang C, Xu XF, Xu W, Liu SW, et al. Structural and functional properties of SARS-CoV-2 spike protein: potential antivirus drug development .Acta Pharmacol Sin. 2020;41(9):1141–1149. doi:10.1038/s41401-020-0485-4.

31 .Spinello A, Saltalamacchia A, Magistrato A. Is the rigidity of SARS-CoV-2 spike receptor-binding motif the hallmark for its enhanced infectivity? Insights from all-atom simulations.

J Phys Chem Lett. 2020;11(12):4785–4790. doi:10.1021/acs.jpclett.0c01148.

32 .Ali A, Vijayan R. Dynamics of the ACE2–SARS-CoV-2/SARS-CoV spike protein interface reveal unique mechanisms. Biophys J. 2020;118(9):2564–2575. doi: 10.1016/j.bpj.2020.03.027

33 .Verkhivker GM. Molecular simulations and network modeling reveal an allosteric signaling in the SARS-CoV-2 spike protein receptor-binding domain: Implications for infectivity and neutralizing antibodies. J Phys Chem B. 2020;124(49):11123–11138. doi: 10.1021/acs.jpcb.0c07209

34 .Golcuk M, Yildiz A, Gur M, et al. Omicron BA.1 and BA.2 variants increase the interactions of SARS-CoV-2 spike glycoprotein with ACE2: insights from molecular dynamics simulations. J Mol Graph Model. 2022;117:108286. doi:10.1016/j.jmgm.2022.108286.

35 .Luan B, Huynh T. In silico antibody mutagenesis for optimizing binding to SARS-CoV-2 spike protein. J Phys Chem Lett. 2021;12(8):2837–2842. doi:10.1021/acs.jpclett.1c00460.